PLOS ONE

Pathological and Molecular Responses around Deep Brain Stimulation Electrodes in MRI Scanning at 1.5-T, 3.0-T and 7.0-T: An In Vivo Comparative Study

--Manuscript Draft--

Manuscript Number:	
Article Type:	Research Article
Full Title:	Pathological and Molecular Responses around Deep Brain Stimulation Electrodes in MRI Scanning at 1.5-T, 3.0-T and 7.0-T: An In Vivo Comparative Study
Short Title:	An In-vivo Study of MRI-related DBS Heating
Corresponding Author:	Jian-Guo Zhang Beijing Tiantan Hospital, Capital Medical University Beijing, CHINA
Keywords:	Deep brain stimulation; MRI; MRI-induced DBS heating; In vivo; Pathology; Heat shock protein.
Abstract:	Objective: The purposes of this study are to investigate the pathological and molecular responses of the tissue surrounding the deep brain stimulation (DBS) electrodes in MRI scanning at 1.5-T, 3.0-T and 7.0-T. Materials and Methods: The PINS DBS devices, a new type of DBS system, were stereotactically implanted into the brains of New Zealand rabbits, targeting the left nucleus ventralis posterior thalami, while on the right side a puncture passage pointing to the same nucleus was made by slowly withdrawing the lead after insertion. MR scanning of routine sequences at multiple levels (1.5-T, 3.0-T and 7.0-T) was performed using the transmit/receive head coils. The responses of the surrounding tissue were evaluated by hematoxylin and eosin staining (H&E staining) and transmission electron microscopy (TEM). The amount of the 70k Da heat shock protein (HSP-70) was quantified by western blot and quantitative polymerase chain reaction (QPCR) to further evaluate the injury. Results: H&E staining and TEM showed that the injury around the DBS electrode was indistinctive to that of the control group ($p > 0.05$). The differences of the pathological alterations among MRI groups were also insignificant ($p > 0.05$). Besides, western blot and QPCR failed to show significant differences between the DBS side and the puncture side in each group ($p > 0.05$). Conclusions: Based on these results, we speculated that MRI at different levels did not induce morphologically observable and molecularly detectable heating injury to the brain tissue surrounding the DBS lead. Although no extrapolation could be made to human tests due to the anatomical differences, these preliminary data furthered our understanding of the MRI-related implant heating and encouraged future investigations on human subjects.
Order of Authors:	Lin Shi
	An-Chao Yang
	Da-Wei Meng
	Huan-Guang Liu
	Shao-Wu Li
	Xin Zhang
	Jian-Guo Zhang
Suggested Reviewers:	Frank G Shellock, MD Keck School of Medicine, Los Angeles, CA frank.Shellock@gte.net
	Devashish Shrivastava, MD Center for Magnetic Resonance Research, University of Minnesota dev@cmrr.umn.edu

Opposed Reviewers:	Ji-Zong Zhao Beijing Tiantan Hospital, Capital Medical University There are several points of conflicted interests with Prof. Ji-Zong Zhao.
Additional Information:	
Question	**Response**
Competing Interest For yourself and on behalf of all the authors of this manuscript, please declare below any competing interests as described in the "PLoS Policy on Declaration and Evaluation of Competing Interests." You are responsible for recognizing and disclosing on behalf of all authors any competing interest that could be perceived to bias their work, acknowledging all financial support and any other relevant financial or competing interests. If no competing interests exist, enter: "The authors have declared that no competing interests exist." If you have competing interests to declare, please fill out the text box completing the following statement: "I have read the journal's policy and have the following conflicts" * typeset	The authors have declared that no competing interests exist.
Financial Disclosure Describe the sources of funding that have supported the work. Please include relevant grant numbers and the URL of any funder's website. Please also include this sentence: "The funders had no role in study design, data collection and analysis, decision to publish, or preparation of the manuscript." If this statement is not correct, you must describe the role of any sponsors or funders and amend the aforementioned sentence as needed. * typeset	This project is supported by the National Natural Science Funds for Distributed Young Scholars, Grant No. 81200997. The funders had no role in study design, data collection and analysis, decision to publish, or preparation of the manuscript.
Ethics Statement All research involving human participants	This study was performed between 8 am and 3 pm and was in accordance with the recommendations from the Guidelines for Use and Care of Experimental Animals, as approved by the Beijing Association on Laboratory Animal Care (Permit Number:

must have been approved by the authors' institutional review board or equivalent committee(s) and that board must be named by the authors in the manuscript. For research involving human participants, informed consent must have been obtained (or the reason for lack of consent explained, e.g. the data were analyzed anonymously) and all clinical investigation must have been conducted according to the principles expressed in the Declaration of Helsinki. Authors should submit a statement from their ethics committee or institutional review board indicating the approval of the research. We also encourage authors to submit a sample of a patient consent form and may require submission of completed forms on particular occasions. All animal work must have been conducted according to relevant national and international guidelines. In accordance with the recommendations of the Weatherall report, "The use of non-human primates in research" we specifically require authors to include details of animal welfare and steps taken to ameliorate suffering in all work involving non-human primates. The relevant guidelines followed and the committee that approved the study should be identified in the ethics statement. Please enter your ethics statement below and place the same text at the beginning of the Methods section of your manuscript (with the subheading Ethics Statement). Enter "N/A" if you do not require an ethics statement.	SYXK 2010-0141). The entire surgery was conducted under urethane anesthesia. Every effort was made to minimize suffering during the procedure.

*Cover Letter

Dear Editors of Plos One editorial staff:

This is an original research article entitled “Pathological and Molecular Responses around Deep Brain Stimulation Electrodes in MRI Scanning at 1.5-T, 3.0-T and 7.0-T: An In Vivo Comparative Study”, written by Dr. Lin Shi and Dr. An-Chao Yang. Previous work has observed temperature changes of the DBS lead during MRI. This study explored the response of the tissue and provided the first data concerning the pathological and molecular alterations around the implanted DBS lead during MRI scanning. Our work is preliminary but thought-provoking because the results implied the heating was not as serious as imagined. Thus it provided evidence for reconsideration of the issue that patients with DBS devices are prohibited from taking ultrahigh field MRI scanning in clinical practice. With great respect, we would like to submit our work to your journal for consideration of publication, because we believe the paper may be of particular interest to the readers of your journal. Neither the entire paper nor any part of its content has been published or accepted elsewhere, nor has it been submitted to any other journal. This manuscript has no conflict of interest. This study was conducted under strict ethical considerations and was permitted by the Laboratory Animal Center of Military Medical Science Academy. Correspondence should be addressed to Prof. Jian-Guo Zhang at the following address, phone and fax number, and email address: Functional and stereotactic laboratory, Beijing Neurosurgical Institute, Tiantan West No. 6, Dongcheng Dist., Beijing, China. Zip code: 100050. Phone: +86-10-67096767. Fax: +86-10-67097507. E-mail address: 173874447@qq.com.

Thanks very much for your attention to our paper.

Best Regards.

Yours Sincerely.

Jian-Guo Zhang

2013-11-14

Pathological and Molecular Responses around Deep Brain Stimulation Electrodes in MRI Scanning at 1.5-T, 3.0-T and 7.0-T: An In Vivo Comparative Study

Lin Shi[1☆], An-Chao Yang[2☆], Da-Wei Meng[2], Shao-Wu Li[1], Huan-Guang Liu[2], Xiu Wang[2], Xin Zhang[1], Jian-Guo Zhang[1 2]*

[1] Beijing Neurosurgical Institute, Capital Medical University, Beijing, China.

[2] Department of Neurosurgery, Beijing Tiantan Hospital, Capital Medical University, Beijing, China.

* Corresponding to: Jian-Guo Zhang, MD, Beijing Neurosurgical Institute, Tiantan West No.6, Dongcheng Dist., Beijing, China. Zip code: 100050. Tel: +86 10 67096767. Fax: +86 10 67097507. E-mail address: zjguo73@126.com.
☆ Lin Shi and An-Chao Yang contributed equally to this article.
Supported by: National Natural Science Funds for Distributed Young Scholars, Grant No. 81200997.

Abstract

Objective: The purposes of this study are to investigate the pathological and molecular responses of the tissue surrounding the deep brain stimulation (DBS) electrodes in MRI scanning at 1.5-T, 3.0-T and 7.0-T.

Materials and Methods: The PINS DBS devices, a new type of DBS system, were stereotactically implanted into the brains of New Zealand rabbits, targeting the left nucleus ventralis posterior thalami, while on the right side a puncture passage pointing to the same nucleus was made by slowly withdrawing the lead after insertion. MR scanning of routine sequences at multiple levels (1.5-T, 3.0-T and 7.0-T) was performed using the transmit/receive head coils. The responses of the surrounding tissue were evaluated by hematoxylin and eosin staining (H&E staining) and transmission electron microscopy (TEM). The amount of the 70k Da heat shock protein (HSP-70) was quantified by western blot and quantitative polymerase chain reaction (QPCR) to further evaluate the injury.

Results: H&E staining and TEM showed that the injury around the DBS electrode was indistinctive to that of the control group ($p > 0.05$). The differences of the pathological alterations among MRI groups were also insignificant ($p > 0.05$). Besides, western blot and QPCR failed to show significant differences between the DBS side and the puncture side in each group ($p > 0.05$).

Conclusions: Based on these results, we speculated that MRI at different levels did not induce morphologically observable and molecularly detectable heating injury to the brain tissue surrounding the DBS lead. Although no extrapolation could be made to human tests due to the anatomical

RF: radio frequency, MRI: magnetic resonance imaging, SAR: specific absorption rate, DBS: deep brain stimulation, VPN: nucleus ventralis posterior, SE: spin echo, GRE: gradient echo, FLAIR: fluid attenuated inversion recovery, H&E staining: hematoxylin and eosin staining, TEM: transmission electron microscopy, HSP-70: 70kDa heat shock protein, QPCR: quantitative polymerase chain reaction

differences, these preliminary data furthered our understanding of the MRI-related implant heating and encouraged future investigations on human subjects.

Introduction

Deep brain stimulation (DBS) is a surging neurostimulation technique and has attracted much academic attention. Its efficacy has been verified but its safety is still under discussion, especially for the heating in radio frequency (RF) field during magnetic resonance imaging (MRI) [1-3]. Based on numerous investigations, only 1.5-T MRI with RF of 64MHz is considered relatively safe when specific guidelines are followed [4-6]. Any attempts trying to surpass such limitations may expose patients to risks of burning as previously indicated [7, 8].

It is true that confining the MRI field strength to only 1.5-T can be protective to patients [2, 5, 9]. However, many hospitals do not have 1.5-T MRI and their MRI systems at else field strength (1.0-T, 3.0-T, etc.) are excluded, which is unfortunate. Moreover, MRI systems at higher field have many advantages over the routine 1.5-T ones, including higher image quality with higher signal-to-noise ratio, faster scanning speed, unique sequences that require higher static magnetic field, etc. [10, 11]. Thus, the application of higher field MRI to patients with DBS devices seems essential. •

Currently, MRI-induced heating of DBS devices has been studied on multiple levels [5, 9, 12]. It is believed that the heating is an interaction between the DBS lead and the external electromagnetic field. Several mechanisms are involved in such process, including the electromagnetic induction, the circuit resonance and the antenna effect, the last two being substantially important in heat production [6, 13]. The absorbed energy comes mostly from RF resonance [4, 12]. The dosimetric quantity used to evaluate the absorption is specific absorption rate (SAR). SAR is thought to be associated with the magnitude of static magnetic field, the

frequency of RF, the density and electric characteristics of the tissue-implant complex, and some other factors (i.e., $SAR = \frac{\sigma \cdot E^2}{\mu}$, E is the internal electric field, σ is tissue density, μ is tissue conductivity) [14-16]. Thus, when the MRI scanner changes from 1.5-T/64MHz to 3.0-T/128MHz, the SAR and the corresponding heat are likely to have a sharp rise.

However, such estimation of the thermal effects has many defects. First, the equation is an over-simplification of the actual SAR and at times it is not accurate [9, 16]. Second, evaluation of the thermal effects from SAR is unreliable since a myriad of other factors are influencing such process [3, 14, 17, 18] Also, some investigations performed on higher-field systems with higher RF frequency (i.e., 3.0-T/128MHz, 7.0-T/300MHz or higher magnitude) did not detect significant temperature elevation on the implants as calculated from the estimation [19-23]. Additionally, several investigations even found lower temperature changes in 3.0-T/128MHz MRI than in 1.5-T/64MHz MRI [24-26]. Besides, most of the studies concerning the heating were acquired in vitro. The response of neural tissue to the MRI-related heating in ultra-high field MRI remained unexplored [9]. Thus, more data are required to confirm the heating effects of DBS lead in higher field MRI under in vivo conditions.

In consideration of the above, we designed this preliminary in vivo comparative experiment to study the MRI-related DBS heating at ultra-high field strength.

Materials and Methods

Ethics Statements and Animal Grouping

This study was performed between 8 am and 3 pm and was in accordance with the recommendations from the Guidelines for Use and Care of Experimental Animals, as approved

by the Beijing Association on Laboratory Animal Care (Permit Number: SYXK 2010-0141). The entire surgery was conducted under urethane anesthesia (1 mg/kg, i.m., Sigma, St. Louis, MO, USA), and the average anesthesia time was approximately 1 hour. The vital signs (heart rate: 100-120 bpm, respiration rate: 10-14/min, and temperature of anus: 37.5-38.5 °C) were continuously monitored throughout the anesthesia. We kept the temperature of the surgery room and the MR scanning room at 35 °C using the temperature control system in order to lessen the influence of the anesthetics on the core temperature. Every effort was made to minimize suffering during the procedure.

The New Zealand rabbit was used for its easy availability, relative inferiority as well as its brain size large enough for the DBS lead. Forty-eight male adult rabbits (weighing 4.5-6.0 kg), provided by the Laboratory Animal Center of Military Medical Science Academy, were randomized into Group 1 (G1, 7.0-T group, n=12), Group 2 (G2, 3.0-T group, n=12), Group 3 (G3, 1.5-T group, n=12) and Group 4 (G4, control group, n=12). Each group was evenly divided into two subgroups (A and B, n=6) since further processing was different. According to relative studies, six samples per group are statistically sufficient in detecting the differences [27, 28]. The grouping information was shown in Table 1. The experimenters were totally blind to the grouping of rabbits.

DBS Implantation

The PINS DBS system (Model G101, PINS Medical Co. Ltd., Beijing, China, Fig.1) was used in this study, which has been verified of its effectiveness and recently released for clinical use in China as a substitute for the Medtronic DBS devices [29]. Parameters of the PINS DBS

system were shown in Table 2 (the parameters of the DBS lead were very close to that of the Medtronic Model 3389 system). Implantation was performed by a team experienced in DBS procedure, targeting the left nucleus ventralis posterior thalami (VPN), using stereotactic devices for rabbits (David KOPF Instruments, Tujunga, CA, USA), according to the atlas (Fig. 2, A Stereotaxic Atlas of the New Zealand Rabbit's Brain, Ivan Urban, Springfield, Charles C Thomas Publisher, 1972). VPN was chosen because its size and position were in favor of DBS implantation. Stereotactic coordinates of VPN, verified in our pre-test, were 12.0 mm anterior to the posterior fontanel, 4.0 mm lateral to the sagittal suture, and 10.5 mm deep to the dura mater. The extension was tunneled subcutaneously through the neck with the connector placed at the middle of the neck. The extra wire was not winded around the burr hole on the head as some surgeons did in clinical practice. On the contrary, the extra wire was zigzagged fixated on the surface of the stimulator (six to seven folds) with sterilized band in order to reduce the wire located on the head (Fig. 1), which was conducive to reduce the covering of the brain by the artifact in MRI as verified by our pre-test. The stimulator was placed 8-10 cm below the last rib and 6-8 cm beside the spine. The above positioning of extension and stimulator was to simulate the bearing of the DBS device inside the coil during an MRI examination. Paracentesis (puncture) to the same nucleus on the right side of the experimental groups and on both sides of G4A was made by slowly withdrawing the DBS lead after insertion, simulating the mechanical injury of DBS implantation. The wounds were carefully sutured. The electric impedance of the devices was examined to ensure correct connection of the DBS devices and the stimulators were turned off throughout the experiment. Rabbits of G4B underwent general anesthesia for 1 hour without operation.

MRI Scanning

MRI scanning was conducted at levels of 1.5-T, 3.0-T and 7.0-T, using transmit/receive head coils (1.5-T: GE Healthcare, UK; 3.0-T: Siemens, US; 7.0-T: Bruker, Germany). The rabbits were secured in supine position with heads fixed within the head holder, so that their bearing and the relative position between the DBS lead and head would be similar to that used by human during MRI. Three separate runs composed of standard spin echo (SE), gradient echo (GRE) and fluid attenuated inversion recovery (FLAIR) sequences were performed at each magnitude, taking more than 25 minutes. All the required patient weight was entered 50Kg. The whole head averaged SARs for each run (the displayed SAR was corrected for the difference between rabbit and human using the method described by Gorny KR [23, 30]) were 0.24-2.20 W/kg for 1.5-T MRI, 0.44-2.60 W/kg for 3.0-T MRI and 0.52-2.96 W/kg for 7.0-T MRI (Table 3). Only rabbits with precise placement of DBS lead in MRI were included in the following experiments (Fig. 3). After MRI scanning, rabbits were put back to their cages without feeding. Most rabbits awoke within 1 hour. No obvious neurological deficits were found.

Pathology

Twenty-four hours after MRI scanning, an appropriate time point to detect tissue injury and apoptosis [31, 32], rabbits were euthanized and decapitated. The brains were dissected along the puncture passage on a plane vertical to the sagittal axis (Fig.4). Samples near the end of the puncture passages from the anterior halves of the brains were processed for H&E staining. Observation was conducted using a light microscope (Axio imager A2, Carl Zeiss, Germany), at

the distance of 0.1 mm, 1.0 mm, 2.0 mm and 3. 0mm away from the passage (measured by the software of the microscope). At each distance, the overall injury was assessed and scored in five random visual fields by a blinded pathologist, using the criteria shown in Table 4. Tissue blocks of appropriate dimensions from the posterior halves of the brains were processed for TEM, at depth of 8 mm to the dura and at distance of 0.1 mm (immediately adjacent to the passage), 1.0 mm, 2.0 mm and 3.0 mm away from the passage. Ultrathin sections of the samples were observed and pictured using a Hitachi H-7650 electron microscope (Tokyo, Japan). The ultrastructural changes were assessed by the pathologist. The injury of the neurons from each sample was scored in five random visual fields according to the criteria in Table 5. If there were several neurons in one visual field, the worst was scored. The scoring systems in Table4 and Table 5 was designed by pathologists from Beijing Neurosurgical Institue, based on relevant references [33-38]. An increment of 0.5 point was added to the score when the injury was between two items in Table 4 and Table 5.

Measurements of 70k Da Heat Shock Protein (HSP-70) and the mRNA

Five hours after MRI scanning, when HSP-70 is regarded at its peak [39, 40], the rabbits of the B subgroups were euthanized and decapitated. The brains were similarly dissected. The tissue of appropriate amount surrounding the end of the lead and the passage was processed for western blot and QPCR assay (Fig.5). The HSP-70 quantity was determined by western blot using a mouse monoclonal antibody that specifically and exclusively recognizes the stress-induced species of HSP-70 (Abcom, Hong Kong). β -actin was used as a marker to quantify the relative quantity of HSP-70 in the cell. QPCR analysis was performed to quantify

the HSP-70 mRNA. The sequence of the genes that encode HSP-70 was obtained on-line from the public database of NCBI (Gene ID: 100354037). The following gene-specific DNA primers, which were designed to specifically recognize the mRNA of HSP-70 using Primer Premier version 5.0 (PREMIER Biosoft International, California, USA), were used on all rabbit tissue: forward, 5'- ATG GCC AAA GGC ACG GCG -3'; reverse, 5'- GCG GGT TCA GCG CCA CCTG -3'. The mRNA of β-actin was used as a marker RNA to quantify the relative quantity of HSP-70 mRNA: forward, 5'-TGA GAG GGA AAT CGT GCG TGA CAT-3'; reverse, 5'-ACC GCT CAT TGC CGA TAG TGA TGA-3'. The mRNA levels of HSP-70 and β-actin were relatively quantified using a fluorescence detection system (CFX96, BioRad, California, USA). We confirmed that each product made by the primers of the target gene showed a single melting curve.

Statistical Analysis

Quantitative data were presented as Mean±SD (standard deviation). All data were analyzed statistically by One-way ANOVA analysis followed by LSD (least significant difference) test, using SPSS 19.0 software program, and difference was considered significant when $p < 0.05$.

Results

Comparison of Pathological Alterations around the DBS Electrodes

H&E Staining

As shown in Fig. 6 (Panels a, f, k, p), the pathology around the passage was featured by a

central puncture passage with injurious alterations that continuously weakened with distance. In the immediate vicinity of the passage (0.1 mm, Fig. 6, Panels b, g, l, q), severe injury was observed. Red neurons (black circles), ghost cells (rightward black arrows), and vacuolization (black asterisks) were prevalent. Karyorrhexis (upward white arrows) was common. The remaining cells were either swollen (white circles) or evidently pyknotic (downward black arrows). Focal hemorrhage (white asterisks) could be seen. At 1.0 mm (Fig. 6, Panels c, h, m, r), the injury diminished obviously comparing with 0.1 mm, with many evidently pyknotic cells (downward black arrows), swollen cells (white circles), red neurons (black circles) and apoptosis (rightward white arrows). Vacuolization (black asterisk) was less obvious. At 2.0 mm (Fig. 6, Panels d, i, n, s), the injury further declined. Oval lightly-stained swelling cells (white circles) were observed in the granulate matrix adorned with entangled fibers and swollen neuropils (leftward white arrows). Apoptosis (rightward white arrows), pyknotic cells (downward black arrows) and red neurons (black circles) were much less common. Ghost cells were not seen. At 3.0 mm (Fig. 6, Panels e, j, o, t), the injury nearly disappeared. Many angular-shaped neurons with darkly-stained Nissl's bodies were nearly unimpaired, although sporadic apoptosis and mildly pyknotic cells could be found. The very slightly swollen neuropils (leftward white arrows) were beset within the indiscrete extracellular matrix. Besides, the scoring of H&E staining was processed by One-way ANOVA and the data showed that the injury declined with distance in each group. The pathological differences among G1A (L), G2A (L) and G3A (L) were insignificant ($p > 0.05$). Besides, the tissular injury of G1A (L), G2A (L) and G3A (L) was indistinctive to that of G4A (L) ($p > 0.05$) (Fig.7).

Transmission Electron Microscopy

In order to further compare the ultrastructural alterations of the injury around the passage, TEM was conducted at distance of 0.1 mm, 1.0 mm, 2.0 mm and 3.0 mm. The overall injury declined with distance in each group. At 0.1 mm (Fig. 8, Panels a, e, I, j. Magnification × 1.0k), the injury was very severe. Large amount of cracked fragments from disintegrated organelles were observed. Mostly the neurons were obviously pyknotic, some with complete cell membrane and some without. The nuclei were deformed or ruptured. Karyorrhexis and karyolysis was common. The glials (astrocytes and oligodendrocytes) were overwhelmingly swollen, some of which were disintegrated. Cavitated axons with loosened myelin sheath were commonly seen. The structure of blood brain barrier was usually incomplete with huge foot processes of astrocytes and ruptured endothelium. At 1.0 mm (Fig. 8, Panels b, f, j, n. Magnification × 1.0k), the injury was slightly ameliorated. Although lots of cells were still pyknotic, the nuclei were usually deformed but integrated. The proportion of disintegrated cells declined, together with the cracked fragments in extracellular matrix. The glials were still severely swollen, though a little better than 0.1 mm. Some axons were swollen with looming, undissolved neurofilaments. No ruptured capillaries were observed, though some were tumid. At 2.0 mm (Fig. 8, Panels c, g, k, o. Magnification × 0.8-1.0k), the injury was greatly improved since less pyknosis was observed. Swelling of neurons and glials was diminished. In some neurons only proportional endoplasmic reticulum and mitochondria were swollen, and in some astrocytes only decreased electron density was seen. The myelin sheath was still swollen. The capillaries were much less tumid with deformed and stenotic but larger lumens. At 3.0 mm (Fig. 8, Panels d, h, l, p. Magnification × 0.9-1.2k), the injury was much alleviated comparing with the former ones. Only trace swollen could be found in some of the organelles in neurons and glial

cells. Layer-like separation was less evident. The stenosis and deformation of capillaries were slight. Some parts of the samples at this distance could hardly be distinguished from the normal tissue. In addition, the scoring of TEM was processed by One-way ANOVA and showed that the ultrastructural differences among G1A (L), G2A (L) and G3A (L) were insignificant ($p > 0.05$). The tissular injury of G1A (L), G2A (L) and G3A (L) was also indistinctive to that of G4A (L) ($p > 0.05$) (Fig.9).

Expression of HSP-70 surrounding the Passages

Western Blot of HSP-70

To quantify the injury around the passage, HSP-70 was determined by western blot. A representative photo is presented in Fig. 10. After correction to β -actin, the relative levels of HSP-70 in each group was 0.173 ± 0.014 (G1BL), 0.168 ± 0.014 (G1BR), 0.181 ± 0.075 (G2BL), 0.182 ± 0.044 (G2BR), 0.169 ± 0.012 (G3BL), 0.171 ± 0.015 (G3BR), 0.005 ± 0.002 (G4BL), 0.003 ±0.001 (G4BR). The data were statisticall0y processed with One-way ANOVA and shown in Fig. 11. The expression of HSP-70 in the experimental groups were significantly higher than the control group ($p < 0.05$, *). Nevertheless, the variance of HSP-70 between the left side and the right side was not significant in each group ($p = 0.094$ #, 0.854 △, 0.587 □).

QPCR of HSP-70 mRNA.

The HSP-70 mRNA around the electrodes was measured by QPCR. The results were made into a bar graph shown in Fig. 12. After correction to β -actin, the relative levels of HSP-70 mRNA were 0.793 ± 0.024 (G1BL), 0.777 ± 0.019 (G1BR), 0.799 ± 0.036 (G2BL), 0.806 ± 0.022 (G2BR), 0.770 ± 0.016 (G3BL), 0.783 ± 0.012 (G3BR), 0.054 ± 0.020 (G4BL), 0.049 ±

0.025 (G4BR). The expression of the HSP-70 mRNA was significantly higher in the experimental groups than in the control group ($p < 0.05$, *). However, no significant difference was found between the left side and the right side in each group ($p = 0.397$ #, 0.726 △, 0.489 □).

Discussion

In the present investigation, we determined the responses of the surrounding tissue to the heating of DBS lead under different MR systems. Results from the morphological examinations (i.e., H&E staining and TEM) showed that the injury was severe with obvious necrosis in the vicinity of the passage, whereas at 2.0 mm and 3.0 mm the injury gradually diminished. This finding indicated that the influenced range was probably within a scope of several millimeters, which was in accordance with some former mathematical calculations of the distribution of temperature changes around the DBS lead in MRI [12, 41-43]. Besides, semi-quantification of H&E staining and TEM failed to show significant differences across the different groups in this study, suggesting that no "extra" morphological injury was induced around the DBS lead in the experimental groups and the control group, in addition to the mechanical injury.

On the other hand, we also performed molecular examinations to evaluate the injury around the DBS lead since the elevation of the inducible HSP-70 parallels the total injury to the cell [44, 45], even when the injury was mixed or inflicted in two steps [46]. Sometimes the inducible HSP-70 was used as a marker to estimate the overall damage to the cell [45, 47]. Results from western-blot and QPCR showed that no significantly higher levels of HSP-70 comparing with

the contralateral sides ($p > 0.05$), which implied that the elevation of HSP-70 might come from the mechanical injury of DBS implantation. Several studies have measured the temperature changes induced during electromagnetic coupling with MRI, and our results were in accordance with their findings [20, 23, 43]. Based on the above, we propose that in this study MRI at different levels failed to induce observable heating injury around the DBS lead.

Our findings need to be further explained from the following aspects. First, based on former investigations concerning the heating of metal devices including the DBS devices in MRI scanning[3, 26, 48, 49], we think that the DBS leads were not likely to be totally spared from heating during the scanning. Second, previous studies with similar settings and parameters detected minor heating in RF radiation of ultra-high field and frequency [19, 22, 23]. Our data can be considered as a verification from a different aspect. Third, literatures showed that the production of inducible HSP-70 would be triggered when temperature of the cell was above 39-40°C [50], which indicated that in this investigation the induced heat was not enough to raise the temperature of the surrounding tissue to such temperature [23, 51]. Fourth, our findings strongly suggested that the magnetic field and RF frequency might not be playing the most important part in the heating process. Lastly, our findings would be insufficient to absolutely confirm that no heating injury ever existed in this experiment. It was possible that some subcellular injury affecting the functions of organelles occurred without being detected by the examinations we employed. But even if the thermal injury really existed and was not detected by these examinations, we still have reasons to believe that the supposed thermal injury was negligible in this study.

This in vivo study is preliminary and has limitations, primarily for its use of rabbits. The huge

anatomical discrepancies (i.e., the shape, dimensions and others) between human and rabbit makes the findings of this study inapplicable to human subjects. Nevertheless, our study may have important implications to the study of biological responses to the heating of implants in RF radiations in that the thermal conductivities and mass densities of the tissues within rabbit brain are very similar to those of human. Also, our data might be meaningful to future application of MRI scanning on pediatric patients of similar weight with DBS devices and other metal implants. Besides, the results from this study are significant to the exploration of the mechanisms of the heating of DBS devices in MRI scanning. Despite the disadvantages, the easy availability and relative inferiority of rabbits to primates also make it suitable for such a preliminary study.

Our study is further limited in that no direct temperature data were presented. However, this study paid more attention to the morphological and molecular responses and the heating of DBS lead in RF field during MRI has been confirmed by lots of studies. The significance of our study is to provide preliminary in vivo observations of the tissular responses to DBS heating. Other limitations of this study involved the use of general anesthetics during MRI scanning. It is well known that anesthetic agents disrupt cerebral blood flow and reduce the baseline brain temperature [52, 53]. Thus, the influence on the heating of the DBS leads is unpredictable. We monitored and maintained the vital signs at a stable level, and kept the room temperature at 35°C, in order to minimize the influence of general anesthesia. Besides, as previous investigations indicated, the temperature at the DBS electrodes was primarily dominated by the heating of the DBS leads due to the RF radiation and not by the relatively slow changes of the brain metabolism induced by anesthesia [23]. Moreover, our data may also be useful to the sedated or unconscious patients in that the metabolism of the brain is similar [54].

Because of these limitations, the data acquired by our study are insufficient to draw any general conclusions regarding safety of patients with implants during MRI scanning at ultrahigh field strength. In this sense, more studies are needed to study the MRI-induced DBS heating in more generalized conditions.

Conclusions

To our knowledge, this preliminary investigation is the first randomized controlled multi-animal study on the issue of the heating of DBS leads during MRI scanning, and the first in vivo study on the pathological and molecular responses of the brain tissue towards the supposed thermal injury from MRI-induced DBS heating. Results showed that the MRI at different levels failed to induce morphologically observable injury in addition to that from DBS implantation, and no extra HSP-70 synthesis other than that from the mechanical injury was detected. Although it was inappropriate to generalize or extrapolate the conclusions to other experiments in different settings, these preliminary data were encouraging future use of 3.0-T and 7.0-T MRI on patients with implanted neurostimulation devices.

Acknowledgments

The authors wish to thank Prof. Jing-Jun Li, Prof. Yi-Lin Sun and Prof. Fang Luo from Beijing Neurosurgical Institute, for their technical help in the methods of MRI scanning, H&E staining and TEM. We are also indebted to Fellow Jian Wang from Jianxiang Scientific Technique Corp. for his support in the methods of western blot and QPCR.

References

1. Rezai AR, Finelli D, Rugieri P, et al. Neurostimulators: potential for excessive heating of deep brain stimulation electrodes during magnetic resonance imaging. Journal of magnetic resonance imaging : JMRI. 2001;14:488-9.

2. Chhabra V, Sung E, Mewes K, et al. Safety of magnetic resonance imaging of deep brain stimulator systems: a serial imaging and clinical retrospective study. Journal of neurosurgery. 2010;112:497-502. doi:10.3171/2009.7.JNS09572.

3. Rezai AR, Baker KB, Tkach JA, et al. Is Magnetic Resonance Imaging Safe for Patients with Neurostimulation Systems Used for Deep Brain Stimulation? Neurosurgery. 2005;57:1056-62. doi:10.1227/01.NEU.0000186935.87971.2a.

4. Fraix V, Chabardes S, Krainik A, et al. Effects of magnetic resonance imaging in patients with implanted deep brain stimulation systems. Journal of neurosurgery. 2010;113:1242-5. doi:10.3171/2010.1.JNS09951.

5. Larson PS, Richardson RM, Starr PA, et al. Magnetic resonance imaging of implanted deep brain stimulators: experience in a large series. Stereotactic and functional neurosurgery. 2008;86:92-100. doi:10.1159/000112430.

6. Dempsey MF, Condon B. Thermal injuries associated with MRI. Clinical radiology. 2001;56:457-65. doi:10.1053/crad.2000.0688.

7. Spiegel J, Fuss G, Backens M, et al. Transient dystonia following magnetic resonance imaging in a patient with deep brain stimulation electrodes for the treatment of Parkinson disease. Case report. Journal of neurosurgery. 2003;99:772-4. doi:10.3171/jns.2003.99.4.0772.

8. Henderson JM, Tkach J, Phillips M, et al. Permanent Neurological Deficit Related to Magnetic Resonance Imaging in a Patient with Implanted Deep Brain Stimulation Electrodes for Parkinson???s Disease: Case Report. Neurosurgery. 2005;57:E1063. doi:10.1227/01.neu.0000180810.16964.3e.

9. Gupte AA, Shrivastava D, Spaniol MA, et al. MRI-related heating near deep brain stimulation electrodes: more data are needed. Stereotactic and functional neurosurgery. 2011;89:131-40. doi:10.1159/000324906.

10. Magland JF, Rajapakse CS, Wright AC, et al. 3D fast spin echo with out-of-slab cancellation: a technique for high-resolution structural imaging of trabecular bone at 7 Tesla. Magnetic resonance in medicine : official journal of the Society of Magnetic Resonance in Medicine / Society of Magnetic Resonance in Medicine. 2010;63:719-27. doi:10.1002/mrm.22213.

11. Zwanenburg JJ, Versluis MJ, Luijten PR, et al. Fast high resolution whole brain T2* weighted imaging using echo planar imaging at 7T. NeuroImage. 2011;56:1902-7. doi:10.1016/j.neuroimage.2011.03.046.

12. Mohsin SA, Sheikh NM, Saeed U. MRI-induced heating of deep brain stimulation leads. Physics in medicine and biology. 2008;53:5745-56. doi:10.1088/0031-9155/53/20/012.

13. Dempsey MF, Condon B, Hadley DM. Investigation of the factors responsible for burns during MRI. Journal of magnetic resonance imaging : JMRI. 2001;13:627-31.

14. Baker KB, Tkach JA, Nyenhuis JA, et al. Evaluation of specific absorption rate as a dosimeter of MRI-related implant heating. Journal of magnetic resonance imaging : JMRI. 2004;20:315-20. doi:10.1002/jmri.20103.

15. Muranaka H, Horiguchi T, Ueda Y, et al. Evaluation of RF heating due to various implants during MR procedures. Magnetic resonance in medical sciences : MRMS : an official journal of Japan Society of Magnetic Resonance in Medicine. 2011;10:11-9.
16. Panagopoulos DJ, Johansson O, Carlo GL. Evaluation of specific absorption rate as a dosimetric quantity for electromagnetic fields bioeffects. PloS one. 2013;8:e62663. doi:10.1371/journal.pone.0062663.
17. Shellock FG. Radiofrequency energy-induced heating during MR procedures: a review. Journal of magnetic resonance imaging : JMRI. 2000;12:30-6.
18. Rezai AR, Finelli D, Nyenhuis JA, et al. Neurostimulation systems for deep brain stimulation: in vitro evaluation of magnetic resonance imaging-related heating at 1.5 tesla. Journal of magnetic resonance imaging : JMRI. 2002;15:241-50.
19. Shrivastava D, Abosch A, Hanson T, et al. Effect of the extracranial deep brain stimulation lead on radiofrequency heating at 9.4 Tesla (400.2 MHz). Journal of magnetic resonance imaging : JMRI. 2010;32:600-7. doi:10.1002/jmri.22292.
20. Carmichael DW, Pinto S, Limousin-Dowsey P, et al. Functional MRI with active, fully implanted, deep brain stimulation systems: safety and experimental confounds. NeuroImage. 2007;37:508-17. doi:10.1016/j.neuroimage.2007.04.058.
21. Newcombe VF, Hawkes RC, Harding SG, et al. Potential heating caused by intraparenchymal intracranial pressure transducers in a 3-tesla magnetic resonance imaging system using a body radiofrequency resonator: assessment of the Codman MicroSensor Transducer. Journal of neurosurgery. 2008;109:159-64. doi:10.3171/JNS/2008/109/7/0159.
22. Sammet CL, Yang X, Wassenaar PA, et al. RF-related heating assessment of extracranial neurosurgical implants at 7T. Magnetic resonance imaging. 2013;31:1029-34. doi:10.1016/j.mri.2012.10.025.
23. Gorny KR, Presti MF, Goerss SJ, et al. Measurements of RF heating during 3.0-T MRI of a pig implanted with deep brain stimulator. Magnetic resonance imaging. 2013;31:783-8. doi:10.1016/j.mri.2012.11.005.
24. Liu Y, Chen J, Shellock FG, et al. Computational and experimental studies of an orthopedic implant: MRI-related heating at 1.5-T/64-MHz and 3-T/128-MHz. Journal of magnetic resonance imaging : JMRI. 2013;37:491-7. doi:10.1002/jmri.23764.
25. Ideta T, Yamazaki M, Kudou S, et al. Investigation of Radio Frequency Heating of Dental Implants Made of Titanium in 1.5 Tesla and 3.0 Tesla Magnetic Resonance Procedure: Measurement of the Temperature by Using Tissue-equivalent Phantom. Nihon Hoshasen Gijutsu Gakkai zasshi. 2013;69:521-8.
26. Baker KB, Tkach J, Hall JD, et al. Reduction of Magnetic Resonance Imaging-related Heating in Deep Brain Stimulation Leads Using a Lead Management Device. Neurosurgery. 2005;57:392-7. doi:10.1227/01.neu.0000176877.26994.0c.
27. Candas F, Gorur R, Haholu A, et al. The effects of clipping on thoracic sympathetic nerve in rabbits: early and late histopathological findings. The Thoracic and cardiovascular surgeon. 2012;60:280-4. doi:10.1055/s-0031-1299573.
28. Rahmani-Cherati T, Mokhtari-Dizaji M, Vajhi A, et al. Endothelial dysfunction in experimental atherosclerosis in the rabbit with extraction of instantaneous changes in the arterial wall. The journal of Tehran Heart Center. 2012;7:128-35.
29. Liu HG, Ma Y, Zhang K, et al. Subthalamic deep brain stimulation with a new device in Parkinson's

disease: an open-label trial. Neuromodulation : journal of the International Neuromodulation Society. 2013;16:212-8; discussion 8. doi:10.1111/ner.12050.

30. Gorny KR, Bernstein MA, Felmlee JP, et al. Calorimetric calibration of head coil SAR estimates displayed on a clinical MR scanner. Physics in medicine and biology. 2008;53:2565-76. doi:10.1088/0031-9155/53/10/008.

31. Umschwief G, Shein NA, Alexandrovich AG, et al. Heat acclimation provides sustained improvement in functional recovery and attenuates apoptosis after traumatic brain injury. Journal of cerebral blood flow and metabolism : official journal of the International Society of Cerebral Blood Flow and Metabolism. 2010;30:616-27. doi:10.1038/jcbfm.2009.234.

32. Rink A, Fung KM, Trojanowski JQ, et al. Evidence of apoptotic cell death after experimental traumatic brain injury in the rat. The American journal of pathology. 1995;147:1575-83.

33. Wang Q, Huang J, Ma K, et al. Evaluation of ghost cell survival in the area of radiofrequency ablation. PloS one. 2012;7:e53158. doi:10.1371/journal.pone.0053158.

34. Yildirim E, Kaptanoglu E, Ozisik K, et al. Ultrastructural changes in pneumocyte type II cells following traumatic brain injury in rats. European journal of cardio-thoracic surgery : official journal of the European Association for Cardio-thoracic Surgery. 2004;25:523-9. doi:10.1016/j.ejcts.2003.12.021.

35. Wang Y, Ye Z, Hu X, et al. Morphological changes of the neural cells after blast injury of spinal cord and neuroprotective effects of sodium beta-aescinate in rabbits. Injury. 2010;41:707-16. doi:10.1016/j.injury.2009.12.003.

36. Rodriguez-Paez AC, Brunschwig JP, Bramlett HM. Light and electron microscopic assessment of progressive atrophy following moderate traumatic brain injury in the rat. Acta neuropathologica. 2005;109:603-16. doi:10.1007/s00401-005-1010-z.

37. Eke A, Conger KA, Anderson M, et al. Histologic assessment of neurons in rat models of cerebral ischemia. Stroke. 1990;21:299-304. doi:10.1161/01.str.21.2.299.

38. Yoshida. A scoring system for histopathologic and immunohistochemical evaluations of uterine leiomyosarcomas. Oncology Reports. 2009;22. doi:10.3892/or_00000493.

39. Kostal V, Tollarova-Borovanska M. The 70 kDa heat shock protein assists during the repair of chilling injury in the insect, Pyrrhocoris apterus. PloS one. 2009;4:e4546. doi:10.1371/journal.pone.0004546.

40. Manzerra P, Brown IR. Time course of induction of a heat shock gene (hsp70) in the rabbit cerebellum after LSD in vivo: involvement of drug-induced hyperthermia. Neurochemical research. 1990;15:53-9.

41. Elwassif MM, Kong Q, Vazquez M, et al. Bio-heat transfer model of deep brain stimulation-induced temperature changes. Journal of neural engineering. 2006;3:306-15. doi:10.1088/1741-2560/3/4/008.

42. Elwassif MM, Datta A, Rahman A, et al. Temperature control at DBS electrodes using a heat sink: experimentally validated FEM model of DBS lead architecture. Journal of neural engineering. 2012;9:046009. doi:10.1088/1741-2560/9/4/046009.

43. Shrivastava D, Abosch A, Hughes J, et al. Heating induced near deep brain stimulation lead electrodes during magnetic resonance imaging with a 3 T transceive volume head coil. Physics in medicine and biology. 2012;57:5651-65. doi:10.1088/0031-9155/57/17/5651.

44. Kharlamov EA, Lepsveridze E, Meparishvili M, et al. Alterations of GABA(A) and glutamate receptor subunits and heat shock protein in rat hippocampus following traumatic brain injury and in posttraumatic epilepsy. Epilepsy research. 2011;95:20-34. doi:10.1016/j.eplepsyres.2011.02.008.

45. Inoue H, Nakagawa Y, Ikemura M, et al. Molecular-biological analysis of acute lung injury (ALI)

induced by heat exposure and/or intravenous administration of oleic acid. Legal medicine. 2012;14:304-8. doi:10.1016/j.legalmed.2012.06.003.

46. Huang QJ, Xu RX, Ke YQ. [Changes of heat-shock protein 70 in the brain of rabbits with craniocerebral missile injury in hot and humid environment]. Di 1 jun yi da xue xue bao = Academic journal of the first medical college of PLA. 2005;25:1270-1, 5.

47. Rejdak K, Kuhle J, Ruegg S, et al. Neurofilament heavy chain and heat shock protein 70 as markers of seizure-related brain injury. Epilepsia. 2012;53:922-7. doi:10.1111/j.1528-1167.2012.03459.x.

48. Ullman M, Vedam-Mai V, Krock N, et al. A pilot study of human brain tissue post-magnetic resonance imaging: information from the National Deep Brain Stimulation Brain Tissue Network (DBS-BTN). NeuroImage. 2011;54 Suppl 1:S233-7. doi:10.1016/j.neuroimage.2010.09.014.

49. Rezai AR, Phillips M, Baker KB, et al. Neurostimulation system used for deep brain stimulation (DBS): MR safety issues and implications of failing to follow safety recommendations. Investigative radiology. 2004;39:300-3.

50. Miller EK, Raese JD, Morrison-Bogorad M. Expression of heat shock protein 70 and heat shock cognate 70 messenger RNAs in rat cortex and cerebellum after heat shock or amphetamine treatment. Journal of neurochemistry. 1991;56:2060-71.

51. Rylander MN, Feng Y, Bass J, et al. Thermally induced injury and heat-shock protein expression in cells and tissues. Annals of the New York Academy of Sciences. 2005;1066:222-42. doi:10.1196/annals.1363.009.

52. Erickson KM, Lanier WL. Anesthetic technique influences brain temperature, independently of core temperature, during craniotomy in cats. Anesthesia and analgesia. 2003;96:1460-6, table of contents.

53. Kahveci FS, Kahveci N, Alkan T, et al. Propofol versus isoflurane anesthesia under hypothermic conditions: effects on intracranial pressure and local cerebral blood flow after diffuse traumatic brain injury in the rat. Surgical neurology. 2001;56:206-14.

54. Shellock FG, Shields CL, Jr. Radiofrequency energy-induced heating of bovine articular cartilage using a bipolar radiofrequency electrode. The American journal of sports medicine. 2000;28:720-4.

Figure Legends

Figure 1. PINS DBS device and the placement in rabbits. (A) PINS DBS device, Model G101, including stimulator, extension and lead. **(B)** Controller and personal digital assistant for PINS DBS device. **(C)** The stimulator of PINS DBS device with zigzagged wire on its surface. **(D)** Placement of the PINS DBS device in rabbits.

Figure 2. Stereotactic atlas of the rabbit brain. The axial section of the rabbit brain showed the position of VPN. VPN: nucleus ventralis posterior thalami.

Figure 3. MRI (sagittal and axial sections) at levels of 7.0-T, 3.0-T and 1.5-T. This image demonstrated the position of the lead (leftward, black arrow) which was covered by the artifact of the lead and the puncture passage (rightward, white arrow) which was unclear in 3.0-T and 1.5-T images.

Figure 4. Processing of the brains for H&E staining and TEM. The brains were dissected along the puncture passage on a plane vertical to the sagittal axis. From the anterior half of the hemisphere, samples of appropriate dimensions around the end of the passage were obtained and processed for H&E staining. Tissue blocks from the posterior half were processed for TEM at the distance of 0.1 mm, 1.0 mm, 2.0 mm and 3.0 mm away from the passage. HE: H&E staining. TEM: transmission electron microscopy. A: anterior. P: posterior. L: left. R: right.

Figure 5. Processing of the brains for western blot and QPCR. Brains were dissected along the puncture passage on a plane vertical to the sagittal axis. The tissue of appropriate amount surrounding the end of the lead passage was processed for western blot and QPCR assay. WB: western blot. QPCR: quantitative reverse transcription polymerase chain reaction. A: anterior, P: posterior, L: left, R: right.

Figure 6. H&E staining of the tissue around the passage. H&E staining was observed in low magnification and in high magnification at distance of 0.1 mm, 1.0 mm, 2.0 mm and 3.0 mm. Low magnification views (Panels a, f, k, p. Magnification × 40) showed pathology around the passage featured by a central puncture with continuously-weakening injurious alterations. 0.1 mm views (Panels b, g, l, q. Magnification × 400) showed extreme injurious pathology: red neurons (black circles), ghost cells (rightward black arrows), vacuolization (black asterisks), karyorrhexis (upward white arrows), swollen cells (white circles), evidently pyknotic cells (downward black arrows) and focal hemorrhage (white asterisks). 1.0 mm views (Panels c, h, m, r. Magnification × 400) showed severe injury with many evidently pyknotic cells (downward black arrows), swollen cells (white circles), red neurons (black circles), apoptosis (rightward white arrows) and vacuolization (black asterisk). 2.0 mm views (Panels d, i, n, s. Magnification × 400) showed moderate injury with oval lightly-stained swelling cells (white circles), swollen neuropils (leftward white arrows), apoptosis (rightward white arrows), pyknotic cells (downward black arrows), red neurons (black circles) and granulate matrix adorned with entangled fibers. 3.0 mm views (Panels e, j, o, t. Magnification × 400) showed mild injury, unimpaired angular-shaped neurons with darkly-stained Nissl's bodies, mildly pyknotic cells, slightly swollen neuropils (leftward white arrows) and indiscrete extracellular matrix. (L): left side. P (black): puncture.

Figure 7. Injury scoring bar graph for H&E staining of the tissue around the passage. H&E staining of the tissue around the passage was evaluated and scored at distance of 0.1 mm, 1.0 mm, 2.0 mm and 3.0 mm, each with five different visual fields. The data were processed with One-way ANOVA. Results showed that the injury declined with distance in each group. The pathological differences among G1A (L), G2A (L) and G3A (L) were insignificant ($p > 0.05$). Besides, the tissular injury of G1A (L), G2A (L) and G3A (L) was indistinctive to that of G4A (L) ($p > 0.05$). (L): left side.

Figure 8. TEM of the tissue around the passage. TEM was conducted at distance of 0.1 mm, 1.0 mm, 2.0 mm and 3.0 mm. At 0.1 mm (Panels a, e, I, j. Magnification × 1.0k), the injury was generally very severe. Mostly the neurons were obviously pyknotic, some with complete cell membrane and some without. The nuclei were deformed or ruptured. Karyorrhexis and karyolysis was common. At 1.0 mm (Panels b, f, j, n. Magnification × 1.0k), the injury was slightly ameliorated. Although lots of neurons were still pyknotic, the nuclei were usually deformed but integrated. The proportion of disintegrated neurons declined. At 2.0 mm (Panels c, g, k, o. Magnification × 0.8-1.0k), the injury was greatly improved since less pyknosis was observed. Swelling of neurons was diminished. In some of the neurons only proportional endoplasmic reticulum and mitochondria were swollen. At 3.0 mm (Panels d, h, l, p. Magnification × 0.9-1.2k), the injury was much alleviated comparing with the former ones. Only trace swollen could be found in some of the organelles in neurons. (L): left side.

Figure 9. Injury scoring bar graph for TEM of the tissue around the passage. TEM of the tissue around the passage was scored at distance of 0.1 mm, 1.0 mm, 2.0 mm and 3.0 mm. The data were statistically processed and results showed that the ultrastuctural differences among G1A (L), G2A (L) and

G3A (L) were insignificant ($p > 0.05$). The tissular injury of G1A (L), G2A (L) and G3A (L) was also indistinctive to that of G4A (L) ($p > 0.05$). (L): left side.

Figure 10. Western blot bands of HSP-70. Western blot bands of the tissue surrounding the passage in each group showing the quantity of HSP-70 and β -actin. (L), left side. (R), right side.

Figure 11. Western blot bar graph of HSP-70. Bar graph demonstrating the relative levels of HSP-70 as indicated by western blot. Each histogram represents the Mean ± SD of each group. The expression of HSP-70 in the experimental groups were significantly higher than the control group ($p < 0.05$, *). Nevertheless, the variance of HSP-70 between the left side and the right side was not significant in each group ($p = 0.094$ #, 0.854 △, 0.587 □). (*) $p < 0.05$, versus the control group. (#, △, □) $p > 0.05$, versus the contralateral side. (L), left side. (R), right side.

Figure 12. QPCR bar graph of HSP-70 mRNA. Bar graph demonstrating the relative levels of HSP-70 mRNA as indicated by QPCR. Each histogram represents the Mean ± SD of each group. The expression of HSP-70 genes was significantly higher in the experimental groups than the control group ($p < 0.05$, *). However, no significant difference was found between the left side and the right side in each group ($p = 0.397$ #, 0.726 △, 0.489 □). (*) $p < 0.05$, versus the control group. (#, △, □) $p > 0.05$, versus the contralateral. (L), left side. (R), right side.

Tables

Table 1. Grouping information.

Groups	Subgroups	Procedure	MRI	H&E/TEM	WB/QPCR
G1(n=12)	G1A(n=6), G1B(n=6)	DBS(L), P(R)	7.0-T	G1A(L)	G1B(L/R)
G2(n=12)	G2A(n=6), G2B(n=6)	DBS(L), P(R)	3.0-T	G2A(L)	G2B(L/R)
G3(n=12)	G3A(n=6), G3B(n=6)	DBS(L), P(R)	1.5-T	G3A(L)	G3B(L/R)
G4(n=12)	G4A(n=6), G4B(n=6)	P(L/R, G4A) *	7.0-T	G4A(L)	G4B(L/R)

* Rabbits of group G4B underwent general anesthesia for more than 3 hours without operation.

L: left. R: right. P: paracentesis. G: group. H&E staining: hematoxylin and eosin staining, TEM: transmission electron microscopy, HSP-70: 70kDa heat shock protein, QPCR: quantitative polymerase chain reaction

Table 2. Measurements and settings of the PINS DBS system.

Measurements and Settings of the PINS DBS System			
Stimulator		**Extension and Lead**	
Dimensions (mm)	(47±2)×(52±2)×(11±1)	**Extension Length (mm)**	510±20
Weight (g)	35±3	**Extension Diameter (mm)**	2.5±0.2
Stimulation Output	Off	**Lead Length (mm)**	400±10
Stimulation Mode	Bipolar	**Lead Diameter (mm)**	1.3±0.2
Amplitude (volt)	0	**Electrodes Length (mm)**	1.5±0.1
Impedance (Ω)	>4000	**Electrodes Spacing (mm)**	0.5±0.1
Other Parameters	No Changes	**Distal Tip Distance (mm)**	0.5±0.1

Table 3. Information and Parameters of MRI Scanners.

Magnitude	Manufacturer	Scanner	Coil	Software	Runs	Time	SAR	Frequency
7.0-T	Bruker	ClinScan	H, T/R	Syngo	3	25min	0.24-2.20	300 MHz
3.0-T	Siemens	Verio	H, T/R	Syngo	3	28min	0.44-2.60	124 MHz
1.5-T	GE	Signa HDxt	H, T/R	GE	3	32min	0.52-2.96	64 MHz

H: head. T/R: transmit/receive. SAR: specific absorption rate.

Table 4. The criteria for scoring tissue injury in H&E staining.

Scores	Observation
0	Normal. The cells and extracellular matrix were uninjured.
1	Mildly injured. Slightly swollen cells with decreased protrusions spread in the homogenous extracellular matrix. Pyknotic cells, apoptosis or necrosis was rarely seen.
2	Moderately injured. Oval lightly-stained swelling cells. Increased red neurons, pyknotic cells, apoptosis and necrosis were observed in the granulate matrix adorned with entangled fibers. Neuropils were swollen.
3	Severely injured. Red neurons, pyknotic cells and apoptotic cells were commonly seen. Eosinophilic ghost cells interspersed in structureless matrix with disorganized neuropils and tangling fibers.
4	Deadly injured. Eosinophilic ghost cells and conspicuous coagulative necrosis prevailed. Several pyknotic cells and red neurons interspersed in the cluttered matrix which was filled up with vacuoles left by dead neurons.

H&E staining: hematoxylin and eosin staining.

Minimal increment: 0.5. (Designed by Beijing Neurosurgical Institute, 2012)

Table 5. The criteria for scoring the neuronal injury in TEM.

Scores	Injurious manifestations of the neurons in TEM
0	Basically normal.
1	Slightly injured, focally distended ER, condensed or swollen M, fovea on karyolemma.
2	Mildly injured, general swelling of organelles, clearly decreased cytoplasmic electron density, major depression of karyolemma.
3	Moderately injured, severe swelling of the entire cell, formation of cytoplasmic vacuoles or blebs, evident cell shrinkage, transparent cytoplasm.
4	Severely injured, pyknotic cells with deformed but integrated cell membrane and karyolemma, apoptosis.
5	Near death, pyknotic cells with trace of karyorrhexis or karyolysis; disruption of cell membrane, rupture of karyolemma, disintegration of organelles; apoptotic bodies.

TEM: transmition electron microscopy. M: mitochondria. ER: endoplasmic reticulum.

Minimal increment: 0.5. (Designed by Beijing Neurosurgical Institute, 2012。

Figure1
Click here to download high resolution image

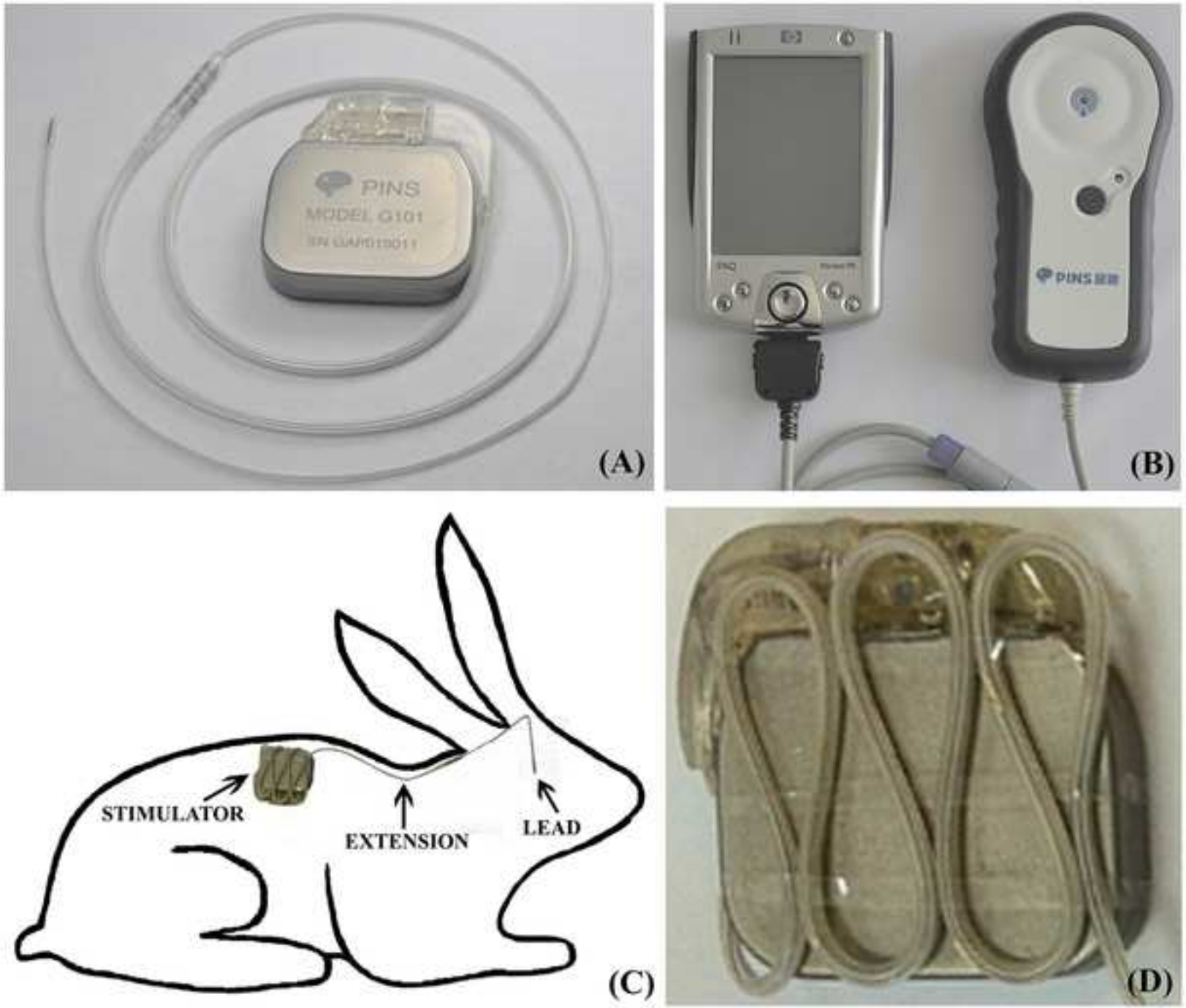

Figure2
Click here to download high resolution image

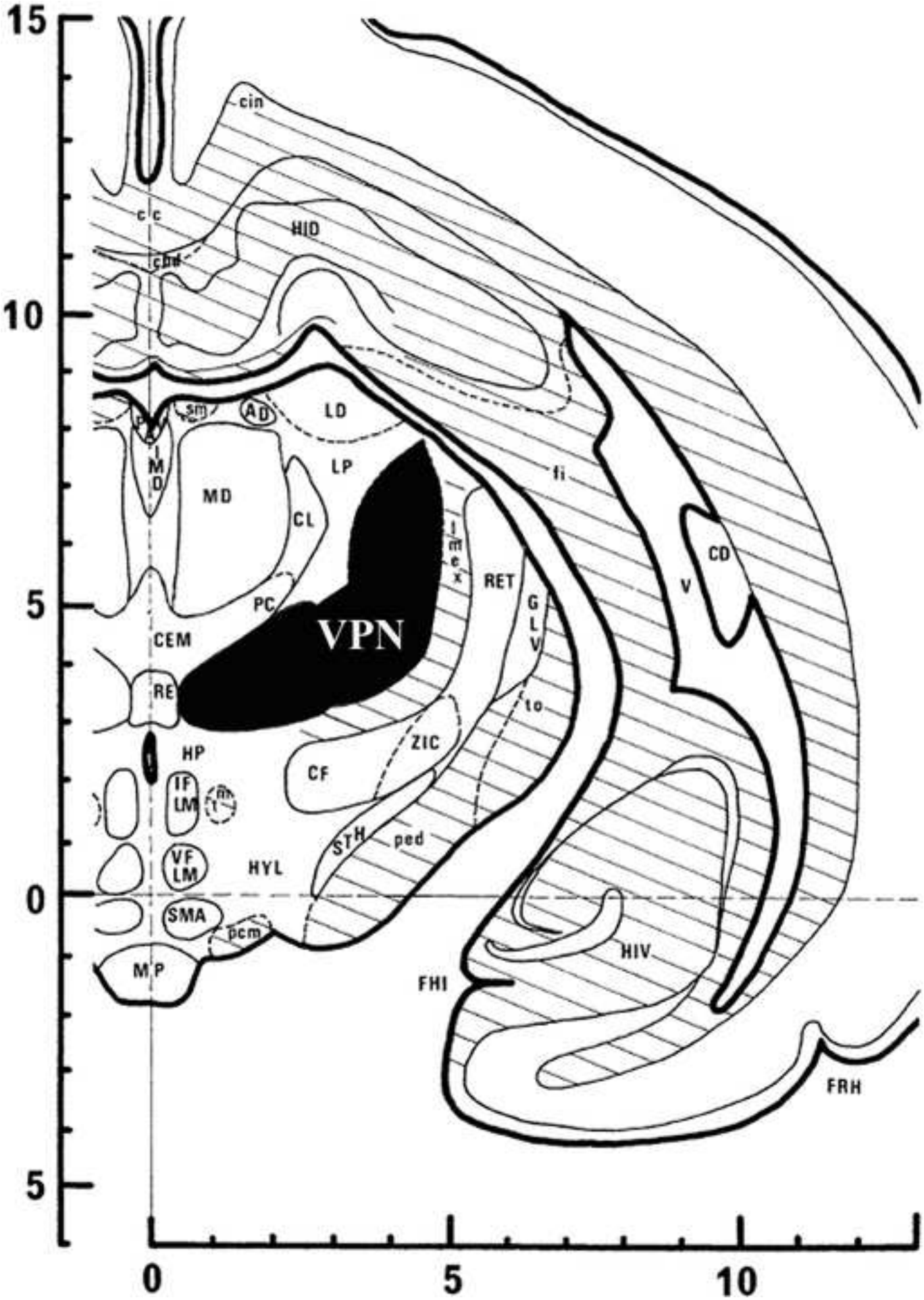

Figure3
Click here to download high resolution image

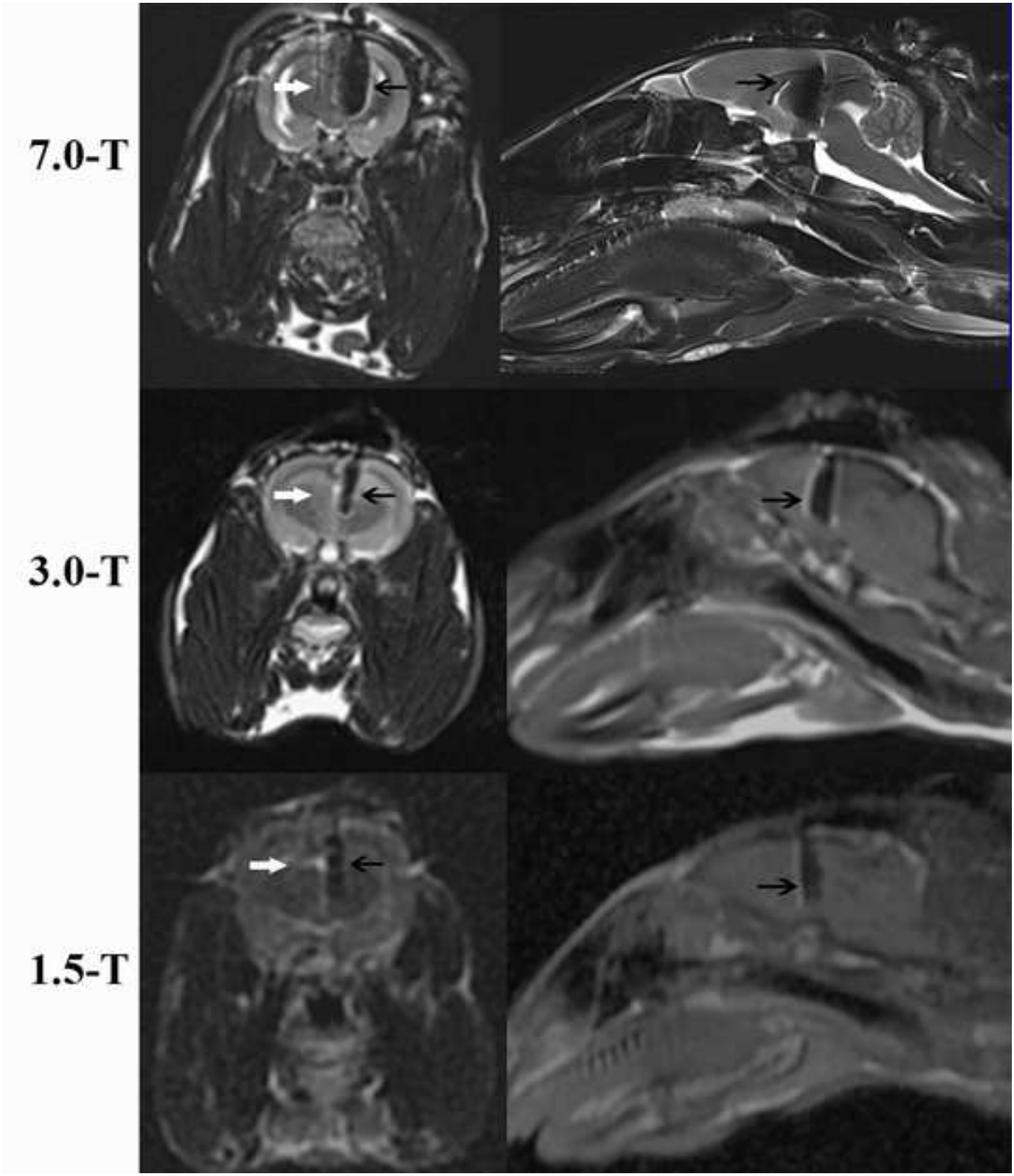

Figure4
Click here to download high resolution image

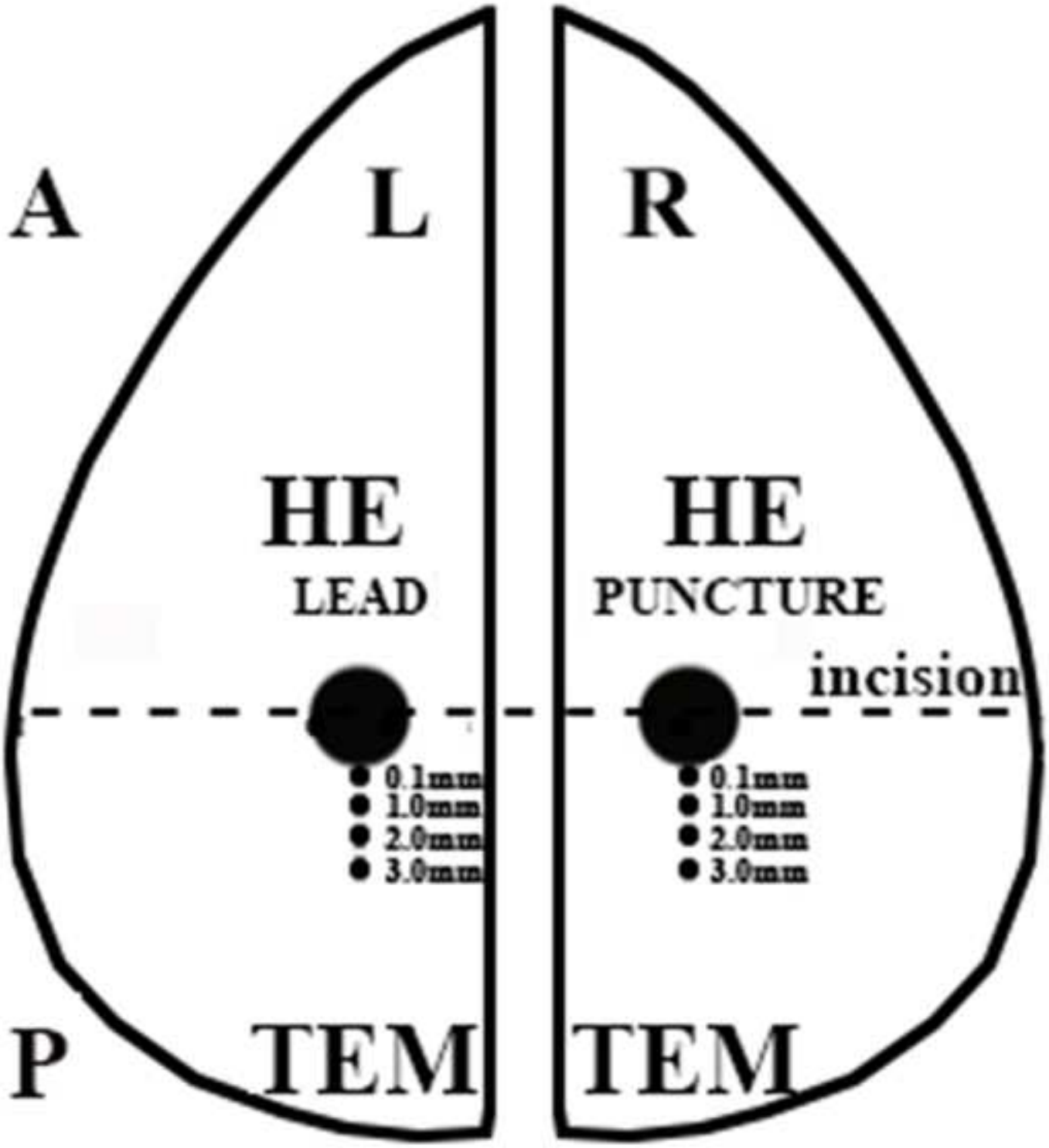

Figure5
Click here to download high resolution image

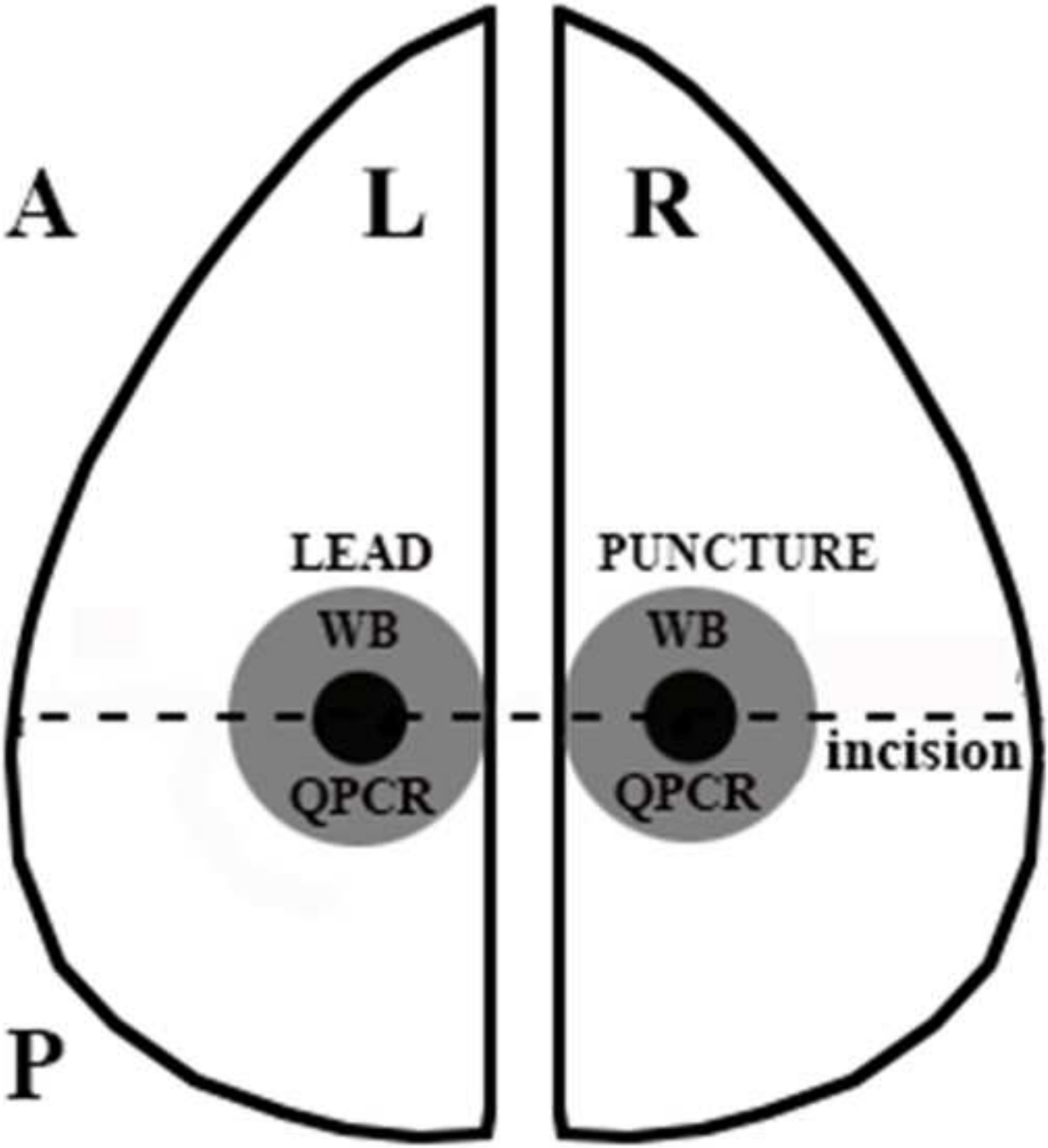

Figure6
Click here to download high resolution image

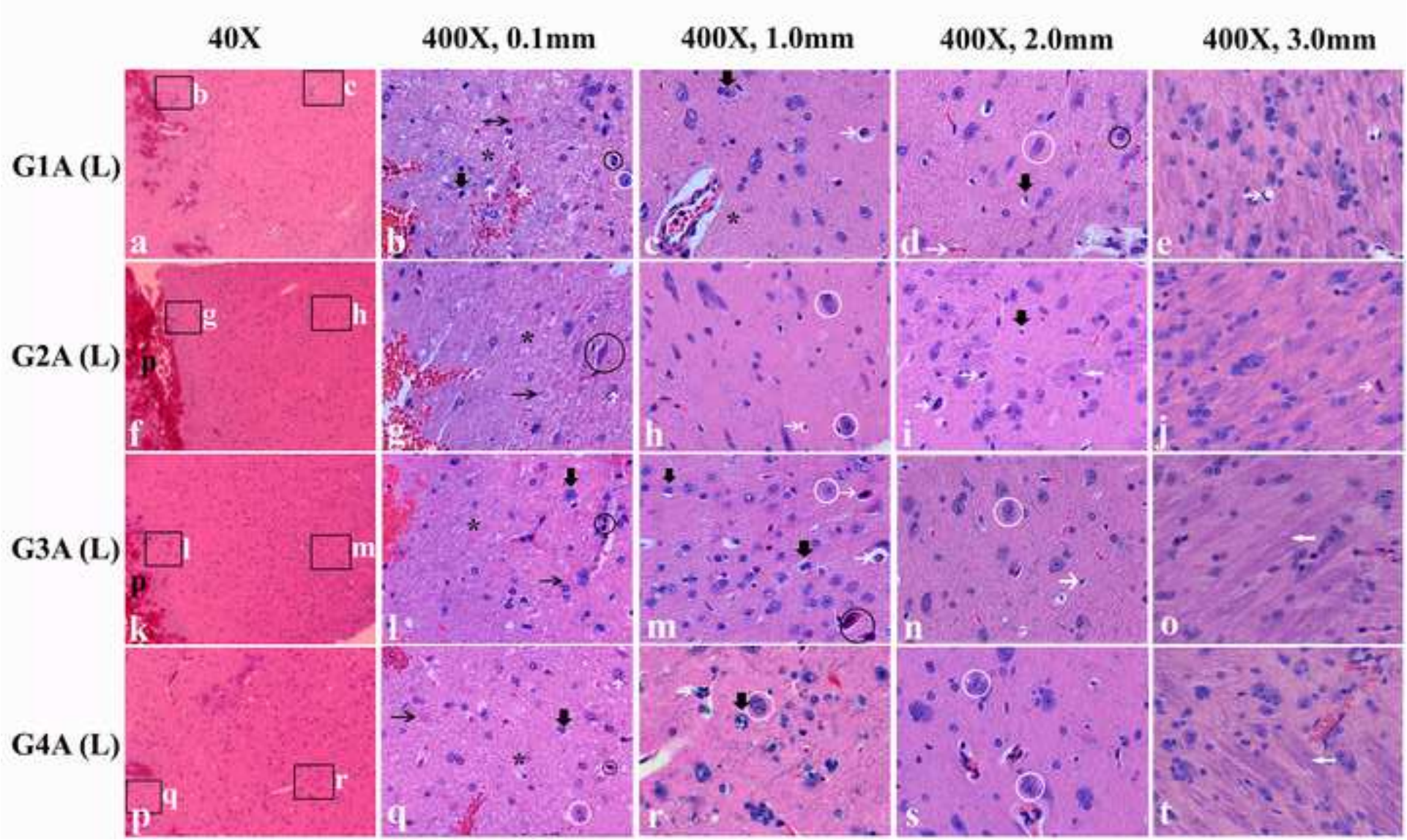

Figure7
Click here to download high resolution image

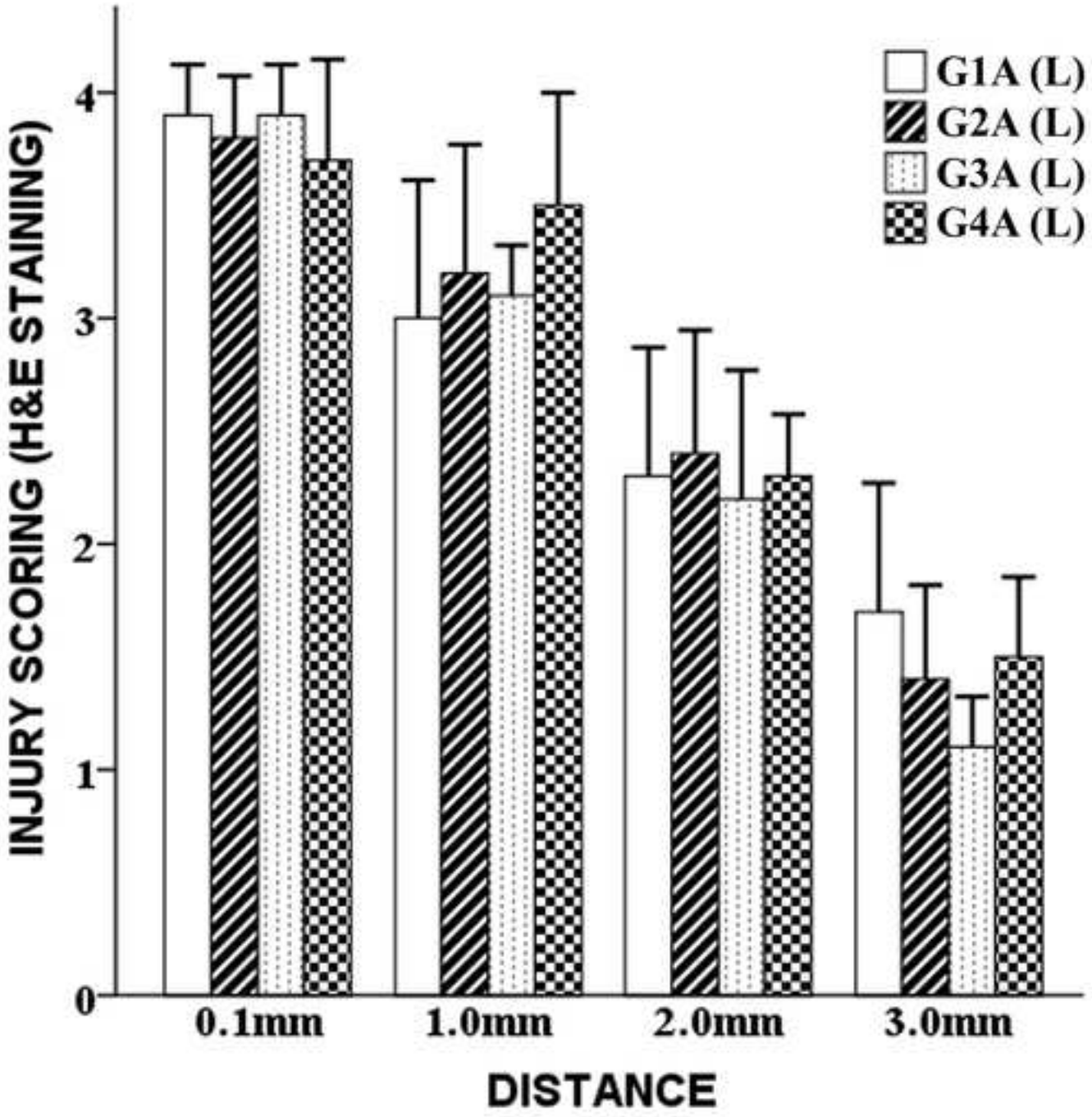

Figure8
Click here to download high resolution image

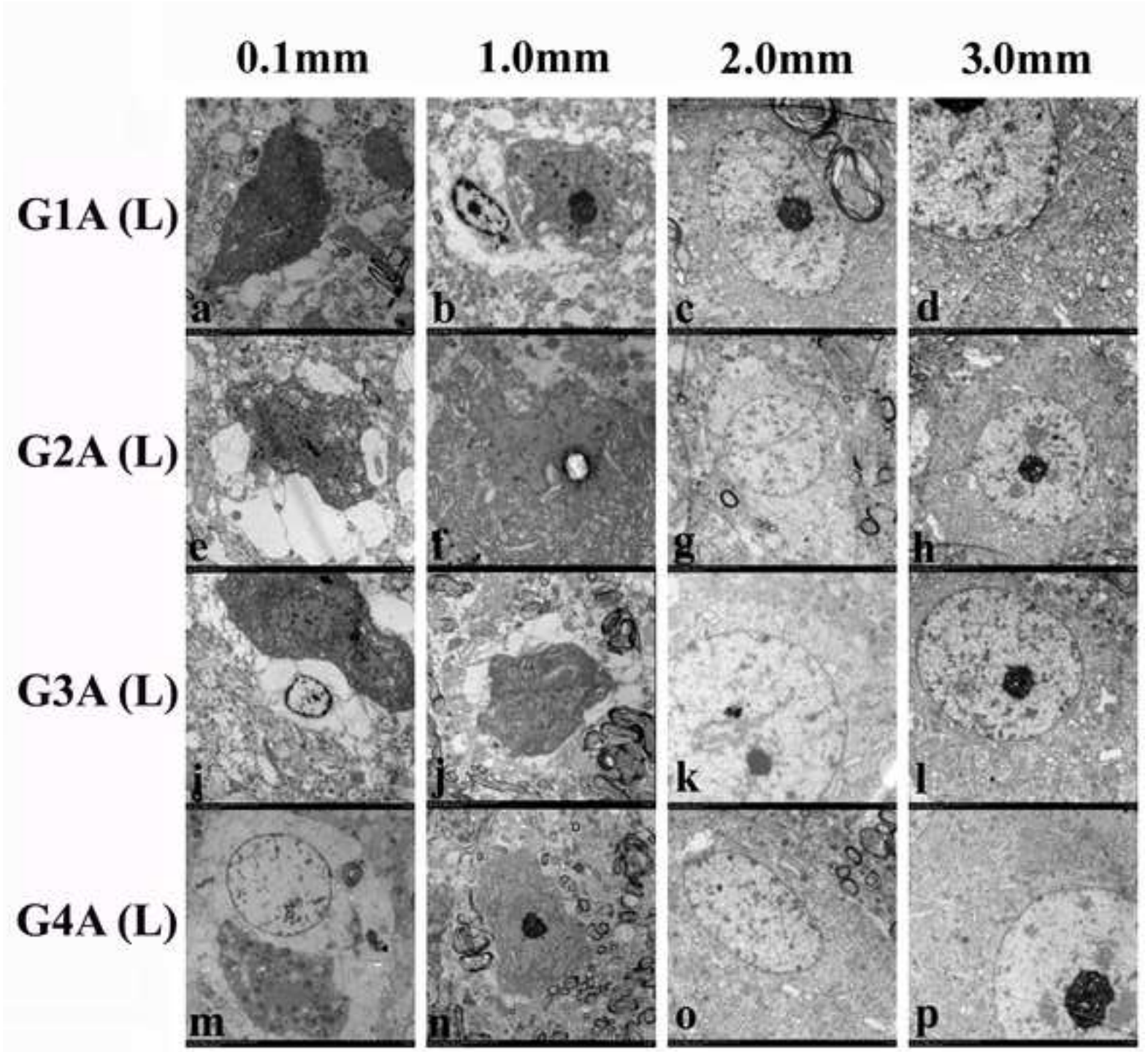

Figure9
Click here to download high resolution image

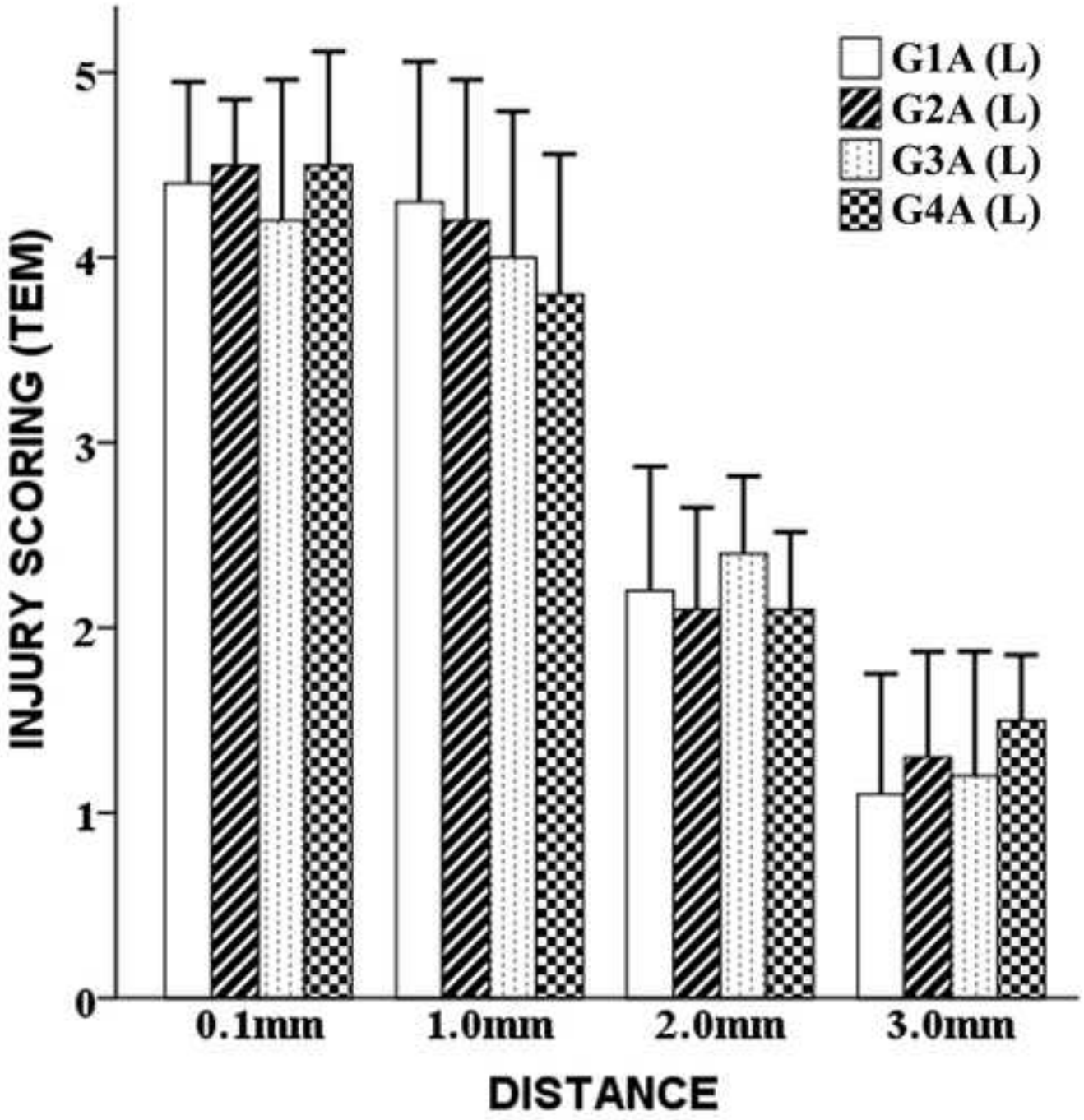

Figure10
Click here to download high resolution image

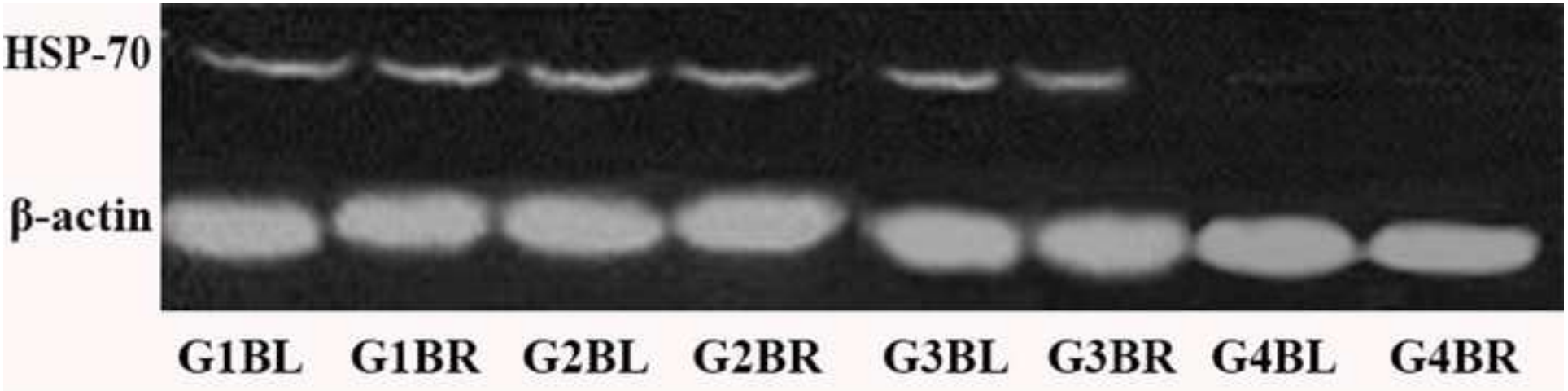

Figure11
Click here to download high resolution image

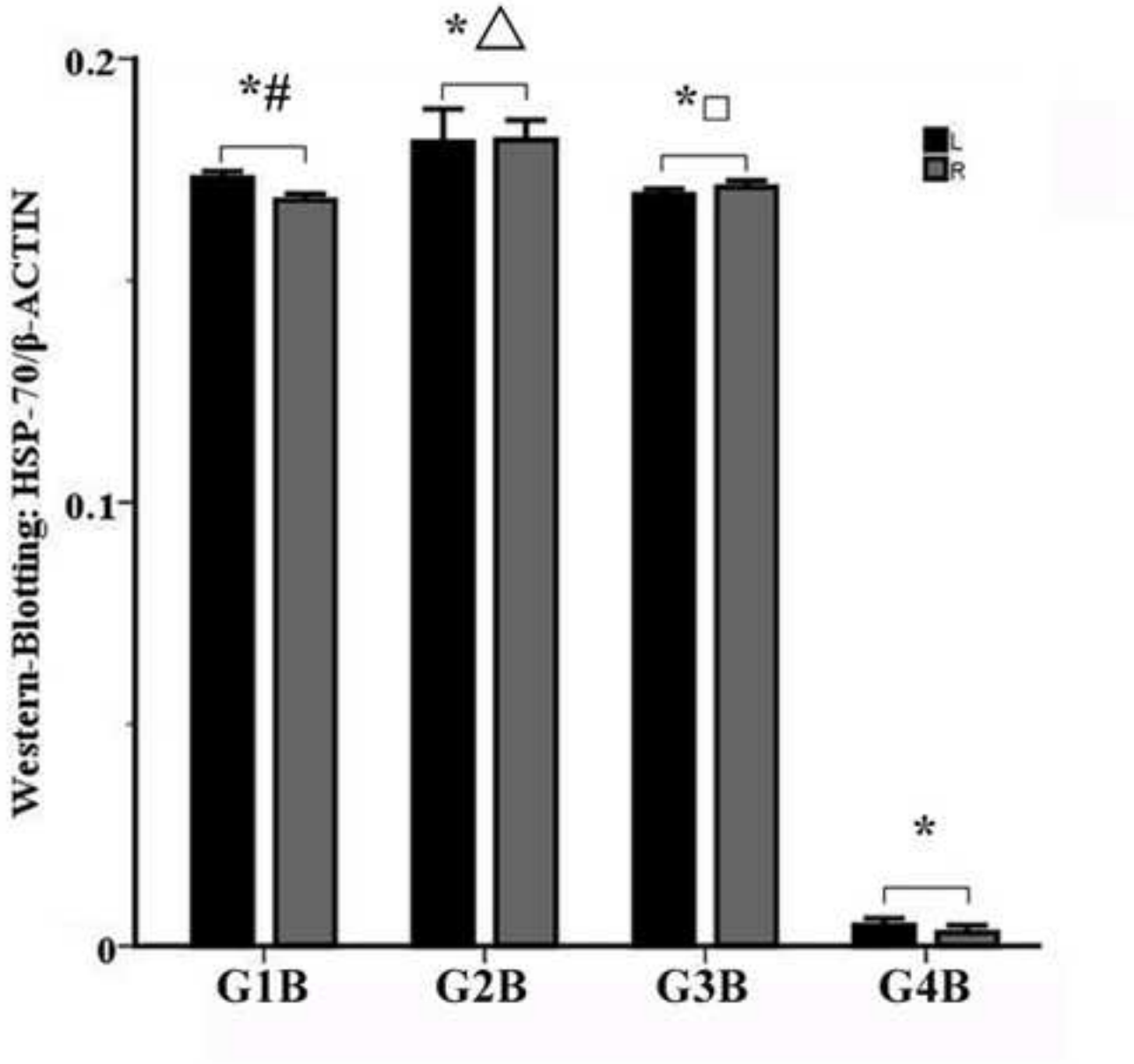

Figure12
Click here to download high resolution image